Simultaneous parametric estimation of shape and impedance of a scattering surface using a multi-frequency fast indirect boundary element method

Yue Li [a,b,*], Jacques Cuenca [a], Laurent De Ryck [a], Mansour Alkmim [a,b], Onur Atak [a], Wim Desmet [b,c], Giulio Dolcetti [d], Anton Krynkin [e]

[a] *Siemens Digital Industries Software, Interleuvenlaan 68, B-3001, Leuven, Belgium*
[b] *Department of Mechanical Engineering, KU Leuven, Celestijnenlaan 300, B-3001, Heverlee, Belgium*
[c] *DMMS Core lab, Flanders Make, Belgium*
[d] *Department of Civil and Structural Engineering, The University of Sheffield, Mappin Street, S1 3JD, Sheffield, UK*
[e] *Department of Mechanical Engineering, The University of Sheffield, Mappin Street, S1 3JD, Sheffield, UK*

ARTICLE INFO

ABSTRACT

Characterization of rough surface properties, such as surface shape or surface impedance, is relevant in many applications. Previous work has been done for characterizing these two aspects separately. This paper proposes a framework for characterizing rough surfaces of finite size in terms of their roughness shape and surface impedance in a single setup. The surface properties are estimated indirectly using a superposition of spatial sinusoidal components for the surface shape and a porous material model for the surface impedance. A fast multipole indirect boundary element method is employed to model the acoustic scattering problem. With the modeling flexibility from the indirect formulation, the target geometry can be simplified as a thin shell representation, which significantly improves computational efficiency. A subtraction method is proposed to mitigate the modeling error of this representation and enable the use of low driving frequencies (e.g. acoustic wavelength is comparable to or larger than the roughness scale) in the characterization. Considering the modeling accuracy of surface shape representation, a discretization criterion concerning both acoustic and spatial aspects is defined. The inverse problem is solved by means of a general-purpose optimizer, minimizing the difference between the simulated and reference acoustic field at multiple driving frequencies. Various numerical examples show that by using reference data with sufficient quality, the proposed framework can retrieve the surface shape and impedance separately, and also simultaneously.

1. Introduction

Acoustic scattering can be utilized for noninvasive material characterization including surface impedance characterization and surface shape reconstruction in free field. For rough surfaces, i.e., smooth perturbations of an otherwise flat plane [1], the characterization of surface shape, e.g., seafloor, sea waves, and river surfaces [2–6], is of vital importance in many applications such as weather forecast, flood prevention, and geophysical inspection. In these cases, the surface shape can be estimated by fitting an acoustic scattering model onto a measurement of the scattered field using a number of sensors placed in front of the surface

---

of interest [7]. Two approaches for the surface reconstruction are common, namely inverting the boundary integral equations that define the forward problem [1,8–11], or alternatively iterative shape updating by an optimization framework seeking to minimize the difference between the predicted and observed acoustic field [12]. Most of the previous studies rely on approximation approaches such as Kirchhoff approximation [1,9], small perturbation expansion [8], Milder's operator expansion [10], and Rytov approximation [13]. These approximations generally simplify the inversion of the system matrix and are computationally efficient to use. However, the assumptions behind such approximations may yield a loss of accuracy under certain circumstances, e.g., in the near field and/or neglecting multiple scattering. In such scenarios, a more accurate numerical method is required. Another common limitation in existing work is the assumption of fully rigid surfaces, where the surface impedance is not considered. This can be unrealistic for many cases in practice where acoustic impedance plays a role in the scattered field.

In the context of surface impedance characterization, two approaches have been standardized, namely the impedance tube measurement [14] and reverberation chamber measurement [15]. However, they have certain limitations in practice. For instance, the impedance tube can only measure the normal impedance of a small material sample [16], while the reverberation chamber often lacks a perfectly diffuse sound field in the test chambers [17]. Besides, the finite size of the test sample may lead to unrealistic results. Brandão et al. [18] presented an extensive literature review on various techniques of *insitu* impedance characterization. In the category of acoustic field methods (by describing the acoustic field above the sample using mathematical formulations), the classical plane wave and spherical-to-plane wave approximations may lead to significant deviations in the low-frequency range due to the plane wave assumptions. The reflection of spherical waves at planar interfaces [19–21] are widely used in the iterative impedance deduction methods with pressure-particle velocity measurement. However, the evaluation of the formulated integral (e.g. Eq. (12) in Brandão et al. [18]) is not possible in a closed form, thereby making it difficult to use as the basis for an inverse method. An improvement can be achieved by using the mathematical model of Di and Gilbert [22] in the iterative deduction method, which formulated the so-called "q-term" method [23]. Yet, it does not account for the size effect and its accuracy can be largely affected by the locations of the receivers in practice [24]. On the other hand, Müller-Trapet et al. [25] has shown that the indirect Boundary Element Method (BEM) is able to provide detailed and high-quality modeling of the real measurement with low numerical uncertainties. In the discussion of Brandão et al. [26], the BEM results are in fact used as a reference in benchmarking other modeling methods for surface impedance characterization. In addition, the asymptotic methods generally assume an infinite sample size and model setup, which is unrealistic in measurements. The finite size of a sound-absorbing material may lead to inaccurate results when measuring its acoustical properties in free field [27,28].

For a given rough surface, it is likely that both surface impedance and shape are not known at the same time. If the surface yields a small-scale roughness compared to the wavelength, the effects from the surface shape can be estimated by using stochastic or *boss* models [29–31]. In the case where the actual surface shape is sought and the roughness scale is comparable to the wavelength, there seem to be scarce investigations in the literature. Qin et al. [32] attempted to reconstruct both shape and surface impedance simultaneously. However, their study is limited to a single parameter that controls both aspects, which can be hardly applied in practice.

The present study investigates and presents a more generic model inversion framework for the characterization of surface shape and surface impedance, both separately and simultaneously, from the scattered acoustic field retrieved at a linear array of sensors. An indirect BEM is employed to model the acoustic surface scattering problem. The surface properties are estimated indirectly using a superposition of spatial sinusoidal components for the surface shape and a porous material model for the surface impedance. It is should be noted that the present study is constrained to rough surfaces varied along one direction only. With the modeling flexibility from the indirect boundary integral formulation, the target scattering surface can be simplified using a thin shell representation. The effect of the finiteness of the sample is mitigated by means of a calibration procedure, consisting of subtracting the acoustic field for a reference finite flat surface from that of the finite rough surface. However, the conventional BEM may become computationally inefficient when the driving frequency increases as smaller elements are required to discretize the acoustic wave sufficiently. The efficiency concern is particularly acute in the optimization framework as the simulation is normally required to run for many iterations. To overcome this issue, the fast multipole method (FMM) [33] is incorporated to accelerate the indirect BEM, which is commonly known as the fast multipole BEM (FMBEM). It significantly improves the computational efficiency of conventional BEM by utilizing the low-rank properties of the system matrix. The inverse problem is solved by an efficient optimization algorithm SHERPA which uses simultaneous multiple search methods [34]. This is coupled with the FMBEM model to minimize the difference between the simulated and reference acoustic fields.

The content of the paper is organized as follows: First, the fundamentals of the methodology including the indirect FMBEM and the optimization framework are presented. In Section 3, the modeling of the scattering problem is discussed including the impedance modeling and surface shape description. Detailed analysis of numerical aspects is given, covering the computer-aided design (CAD) model, geometry discretization, size effects, and error analysis. Section 4 presents several examples of the characterization of surface impedance using single- and multiple-parameter porous models, and the characterization of surface shape based on synthetic data with additive signal noise. Two examples are given for the characterization of surface impedance and shape simultaneously using the proposed framework. Discussions and conclusions are given in the final section.

2. Methodology

2.1. Acoustic scattering problem

The steady-state acoustic pressure p at any location in a three-dimensional fluid domain V excited by a time harmonic source is governed by the in-homogeneous Helmholtz differential equation

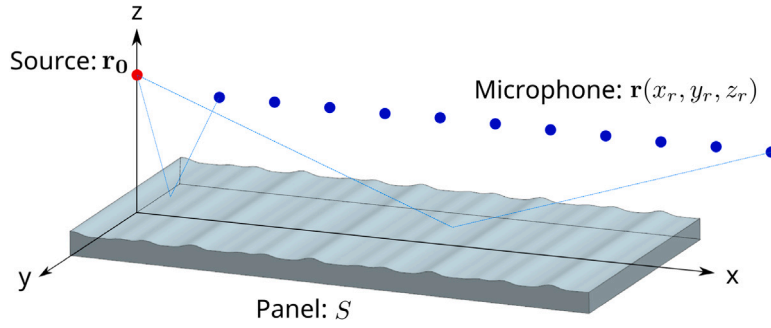$$\nabla^2 p + k^2 p = -\mathrm{i}\omega\rho_0 q(\boldsymbol{r_0}), \tag{1}$$

Fig. 1. Configuration of the surface scattering problem. Both the source and the microphone array are in the $y = 0$ plane.
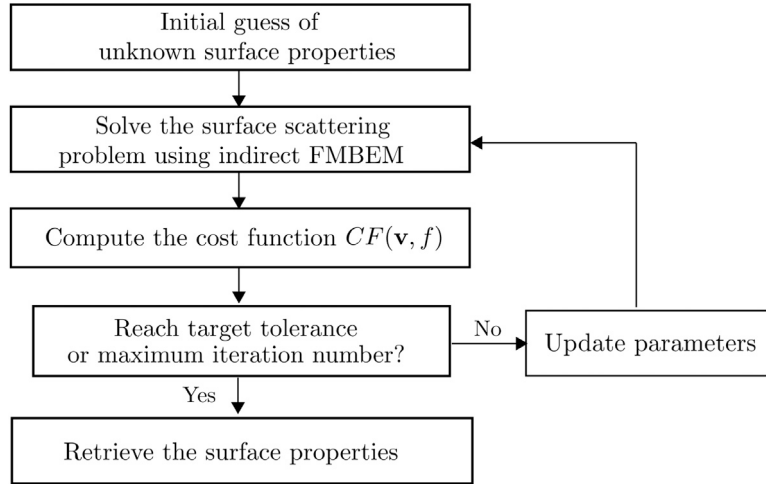

Fig. 2. Parameter estimation flowchart.

where $k = \omega/c$ is the acoustic wave number depending on angular frequency ω and sound speed c, ρ_0 is the fluid density, $q(\mathbf{r_0})$ is the volume velocity of the source at $\mathbf{r_0}$.

The acoustic scattering problem considered here consists of a single acoustic source and a linear microphone array on a plane perpendicular to the surface of interest. Fig. 1 illustrates the configuration of the setup, which replicates the measurement by Dolcetti et al. [1]. This configuration is intended to insonify a large portion of the sample via oblique incidence. It is noted that placing the source within the array would result in a reconstruction of a smaller portion of the sample due to a gap in the microphone array. The surface sample belongs to a panel of finite size in three dimensions. The present study is constrained to the case where the surface elevation varies along x-axis and is constant along y-axis. The source is placed above the sample at $\mathbf{r}_0 = (0, 0, z_0)$. Previous work [1] demonstrated that the effects of the directivity of the source can be incorporated as part of the model. The focus of the present work is on demonstrating the reconstruction in a numerical context and therefore the source is considered punctual. The receivers are also simplified and modeled as omnidirectional point receivers. The sample is assumed to be in the free field. The effect from the floor is thus not considered here, which can be mitigated by adjusting the sample size and directivity of the source in a measurement setup.

In order to estimate the surface properties including surface impedance and/or surface shape, the proposed framework relies on an indirect FMBEM model whose parameters are controlled by a multi-algorithm optimizer. A general workflow is shown in Fig. 2 to demonstrate the characterization process. More details on the solvers are discussed as follows.

2.2. Fast multipole indirect boundary element method

A fast multipole indirect boundary element method is employed to model the surface and the acoustic scattering problem. The basic principle of the indirect boundary integral formulation is recalled here for completeness. The readers are referred to Vlahopoulos [35] for more detailed mathematical derivations.

The indirect boundary integral formulation is derived by using the difference in pressure, i.e., double layer potential μ, and the difference in the normal gradient of the pressure, i.e., single layer potential σ on both sides of the boundary. The pressure at an arbitrary receiver x in space (which could be on the surface or at any microphone position) is induced by an in-homogeneous

free-field pressure from the acoustic source and a homogeneous scattering from points $\boldsymbol{y}$ on the boundary surface S. The scattered pressure is described by the indirect Kirchhoff–Helmholtz integral equation

$$p(\boldsymbol{x}) = \int_S \left[\frac{\partial G(\boldsymbol{x}, \boldsymbol{y})}{\partial n_y} \mu(\boldsymbol{y}) - G(\boldsymbol{x}, \boldsymbol{y})\sigma(\boldsymbol{y}) \right] \mathrm{d}S, \tag{2}$$

where the Green's function in three-dimensional free space is given as

$$G(\boldsymbol{x}, \boldsymbol{y}) = \frac{\mathrm{e}^{\mathrm{i}k|\boldsymbol{x}-\boldsymbol{y}|}}{4\pi \mid \boldsymbol{x} - \boldsymbol{y} \mid}. \tag{3}$$

For the present acoustic scattering problem, the Robin boundary S_Z is used to account for the surface impedance. The single layer potential thus holds a relation with the double layer potential,

$$\sigma(\boldsymbol{y}) = -\mathrm{i}k\beta(\boldsymbol{y})\mu(\boldsymbol{y}), \quad \frac{\partial p(\boldsymbol{y})}{\partial n_y} = -\mathrm{i}k\beta(\boldsymbol{y})p(\boldsymbol{y}), \quad \text{on } S_Z, \tag{4}$$

where the normalized boundary admittance is defined as $\beta = Z_c/Z_s$. $Z_c = \rho_0 c$ is the characteristic acoustic impedance of the fluid, and Z_s is the acoustic impedance of the boundary surface defined in the normal direction. Then the indirect boundary integral formulation (2) can be reformulated as

$$p(\boldsymbol{x}) = \int_{S_Z} \mu(\boldsymbol{y}) \left[\frac{\partial G(\boldsymbol{x}, \boldsymbol{y})}{\partial n_y} + \mathrm{i}k\beta(\boldsymbol{y})G(\boldsymbol{x}, \boldsymbol{y}) \right] \mathrm{d}S_Z. \tag{5}$$

The corresponding pressure gradient can be obtained by taking the normal derivative of Eq. (5). A Galerkin method is applied to the boundary residuals to obtain a variational formulation, which yields

$$\forall(\delta\mu) : \quad \int_{S_Z} R(\mu)\delta\mu \mathrm{d}S_Z = 0, \tag{6}$$

where the residual for the Robin boundary is

$$\begin{aligned} R(\mu) = &\int_{S_Z} \mu(\boldsymbol{y}) \left[\frac{\partial^2 G(\boldsymbol{x}, \boldsymbol{y})}{\partial n_x \partial n_y} + \mathrm{i}k\beta(\boldsymbol{y}) \frac{\partial G(\boldsymbol{x}, \boldsymbol{y})}{\partial n_x} \right] \mathrm{d}S_Z \\ &+ \int_{S_Z} \mu(\boldsymbol{y}) \left[\mathrm{i}k\beta(\boldsymbol{x}) \frac{\partial G(\boldsymbol{x}, \boldsymbol{y})}{\partial n_y} - k^2 \beta(\boldsymbol{x})\beta(\boldsymbol{y})G(\boldsymbol{x}, \boldsymbol{y}) \right] \mathrm{d}S_Z. \end{aligned} \tag{7}$$

The BEM system is formulated and solved by numerical discretization of Eq. (6). The acoustic quantities at microphone positions are then retrieved using Eq. (2) and its normal derivative. The benefit of employing indirect boundary integral formulation in modeling surface scattering problems is that the indirect formulation is valid for problems with open boundary surfaces or thin shell elements, which can be challenging for a commonly used direct boundary integral formulation.

The lack of popularity of BEM for the present application on inverse characterization is due to its high computational cost. The conventional BEM requires $\mathcal{O}(N^2)$ operations to assemble the system matrix, with N being the number of degrees of freedom (Dofs). The actual computational cost becomes high for large models and/or at high frequencies. As a state-of-the-art acceleration method, the FMM [33] is implemented to accelerate the indirect BEM. Essentially, the FMM partitions the BEM system into near-field assemblies and far-field approximations whenever the multipole expansion holds. The latter can significantly reduce the computational cost with controllable numerical accuracy. The overall numerical complexity of FMBEM is typically reduced to $\mathcal{O}(N log^2 N)$. For the detailed numerical implementation of the method, we refer to Fischer [36] and Darve [37,38].

2.3. Parameter estimation methodology

The present characterization problem is formulated as a minimization problem and implemented using numerical optimization. More specifically, by minimizing the defined cost function (CF), the optimizer provides estimations on model parameters that cannot be accessed in a direct manner. For a target parameter vector $\mathbf{v}$, the CF, at a given driving frequency f, is here defined as the root mean square of the normalized difference between the simulated and reference acoustic quantities,

$$CF(\mathbf{v}, f) = \sqrt{\frac{1}{M} \sum_{i=1}^{M} \frac{\left[\gamma_i(f) - \Gamma_i(f) \right]^2}{\mid \Gamma_i(f) \mid}}, \tag{8}$$

where M is the total number of microphones in the setup, γ_i is the simulated response at microphone i, using the parameter values from the optimizer, and Γ_i is the reference response function. The definition of the response functions depends on the modeling method, which will be discussed in detail in Sections 3.2.4 and 3.2.5. In order to avoid an under-determined optimization system, multiple driving frequencies are preferable in the study, which leads to a multi-objective optimization problem. The effects of using a different number of driving frequencies will be discussed in Section 4.2 in detail. The weighting factor for each independent $CF(\mathbf{v}, f)$ is considered to be equal in the present study.

Depending on the problem of interest, the variables to be estimated can be the parameters of geometric shape, surface admittance/impedance, or both. As the search space of the optimization grows exponentially with the number of unknowns, such parameters should be carefully determined to well describe the target problem and to formulate a favorable search space for optimization. In the present characterization study, the objective is to find a parameter vector $\mathbf{v} = \{\alpha_1, \alpha_2, \ldots, \alpha_m, \eta_1, \eta_2, \ldots, \eta_n\}$,

where $\{\alpha_1, \alpha_2, \dots, \alpha_m\}$ is the parameter set of the function to describe the surface shape and $\{\eta_1, \eta_2, \dots, \eta_n\}$ is the parameter set for the porous model used. It should be noted that the chosen parameters may yield inter-dependencies, which should be considered as additional constraints in the optimization. For instance, in the Johnson–Champoux–Allard (JCA) model [39,40], the viscous characteristic length must be equal to or smaller than the thermal characteristic length [41,42]. In general, for each parameter v_i, a corresponding lower bound B_i^l and upper bound B_i^u are defined such that the optimization problem can be written as

$$
\begin{cases}
\text{minimize } CF(\mathbf{v}, f) \\
\text{subject to } B_i^l \leq v_i \leq B_i^u, \quad i \in \{1, 2, \dots, m+n\}.
\end{cases}
\tag{9}
$$

The selection of an appropriate optimizer is dictated by both performance and usability. Non-derivative based algorithms are considered here since they are easy to use and mitigate the implementation effort. Considering the efficiency of simultaneous multiple search methods, the optimization algorithm SHERPA [34] from Simcenter HEEDS [43] is coupled with the FMBEM models to solve the constrained optimization problem. Defining an appropriate convergence criterion poses another challenge. Based on our experience, a two-fold stopping criterion is defined and used in the present study: (1) $CF(\mathbf{v}, f) < 0.05$ for all driving frequencies; (2) a maximum iteration number, e.g. a thousand iterations. This criterion works fine for the chosen optimizer to estimate the parameters with good quality, which is demonstrated in the case studies in Sections 4.1 and 4.2. For a more challenging case with a large search space in Section 4.3, the iteration number can be increased accordingly.

3. Numerical modeling

This section presents the numerical modeling details of the acoustic scattering problem for accurate and efficient characterization. The discussion concerns both impedance and geometry models. For the latter, a simplified thin shell modeling approach is proposed and compared to the volumetric model. A surface discretization criterion is formulated concerning both acoustic and geometric aspects. The size effect and modeling error are also analyzed, and a subtraction method is proposed to mitigate the finite-size effect and thus reduce modeling errors.

3.1. Surface impedance modeling

In the implementation of the FMBEM solver, the surface impedance is defined in the normal direction of the discretized element and is assumed to be constant in space and therefore considered locally reacting. To estimate the frequency dependent impedance, the framework relies on phenomenological porous models to approximate the target material. Therefore the surface impedance is estimated indirectly via the parameters used to describe the material. Various phenomenological models can be used for this purpose. In the present study, we consider both a single-parameter model, i.e., Delany–Bazley–Miki (DBM) model [44], and a multiple-parameter model, i.e., JCA model. The DBM model rather than the original Delany–Bazley model [45] is considered here in order to prevent negative values of the real part of the surface acoustic impedance at low frequencies. As for the characterization of an unknown surface without much *a priori* information on the impedance, it is practical to start with such phenomenological impedance models considering their simplicity and efficiency. Other impedance models can be considered depending on the knowledge of the target surface. The characteristic impedance obtained from the models is then computed as normal impedance to be used in the numerical model and simulation.

3.2. Description of the surface geometry

3.2.1. Rough surface model
The rough surface model considered in this study is based on spatial sinusoidal components. Similar models have been considered in the literature [9,12,46]. The spatial elevation of the surface along the x axis in Fig. 1 is defined as

$$
z(x) = \sum_n z_n \cos\left(\frac{2\pi}{\lambda_n} x + \phi_n\right),
\tag{10}
$$

where z_n, λ_n and ϕ_n are the amplitude, wavelength and phase of the nth sinusoidal component, respectively. An example of such surface using three sinusoidal components is given in Table 1.

3.2.2. CAD modeling
Acoustic scattering on panels of finite dimensions may be subject to size effects [27,28]. The sample size should be considered when using relatively low driving frequencies since waves will diffract around the finite sample. This effect plays a role when one tries to estimate the shape and/or surface impedance at wavelengths comparable to the sample's roughness scale. Such edge diffraction effect can be mitigated using directive high-frequency excitation [1]. In this case, the sample size would become larger than the area insonified by such a source, given its directivity pattern, proper orientation angle, and proper distance to the sample.

A volumetric model, illustrated in Fig. 3(a), accurately represents surface samples such as those used in previous experimental work [1]. However, such a volumetric model increases computational cost and is subject to fictitious interior resonances [47]. This non-physical fictitious resonance is alleviated by an additive impedance boundary condition which is partially assigned to the inner side of the panel [48]. Nevertheless, this extra treatment induces additional computational efforts. Instead, it is here proposed to take advantage of the flexibility of the indirect formulation by modeling the panel as a thin shell with open boundary conditions, as shown in Fig. 3(b). The proposed modeling approach eliminates the efforts on the treatment for fictitious resonances.
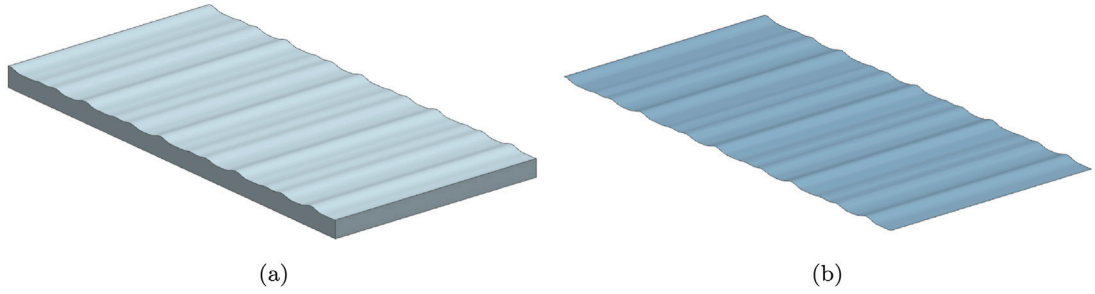
Fig. 3. Examples of the model: (a) full volumetric model; (b) simplified thin shell model.

Table 1
Parameter values for the wavy panel.
Source: Values are adopted from Krynkin et al. [46].

n	z_n [mm]	λ_n [mm]	ϕ_n [rad]
1	1.20	115	−0.46
2	0.81	76.7	−0.08
3	0.49	46	−0.83

Table 2
Comparison of computational efficiency for different geometry models (with rigid surface). The computational time (in minutes) for BEM and FMBEM is averaged over all driving frequencies.

Profile	Model	Elements	Dofs	T_{BEM} [min]	T_{FMBEM} [min]
Flat	Volumetric	62 444	93 668	72.5	10.1
Flat	Thin shell	27 722	14 112	4	0.7
Wavy	Volumetric	63 164	94 748	76	10.5
Wavy	Thin shell	28 054	14 280	4	0.7

3.2.3. Computational efficiency

To evaluate the volumetric and thin shell modeling approaches, a numerical study is conducted as follows. The length, width and mean height of the volumetric model are 500 mm, 250 mm, and 20 mm, respectively. The source is positioned at $z_s = 300$ mm. An array of 35 microphones is deployed in x direction with a linear spacing of 20 mm. The vertical position of the microphone array is $z_r = 300$ mm. Two sets of surface profiles are considered including a flat and a wavy profile. The wavy surface considers the first three sinusoidal components of the surface reported in Krynkin et al. [46] whose parameters are replicated here in Table 1. In order to evaluate the accuracy and efficiency of the two modeling approaches, a wide range of frequencies is covered in this study, i.e. 4 kHz–16 kHz with 0.5 kHz resolution.

Table 2 compares the number of elements from discretization, the number of Dofs in the calculation, and the averaged computational time for different models using conventional indirect BEM (Simcenter 3D [49]) and FMBEM (in-house code under development). All the simulations are conducted on a Windows 10 laptop (Intel i7-7920HQ CPU @3.1 GHz with 32.0 GB memory). In both flat and wavy profiles, the computational efficiency of the thin shell model is significantly faster than the volumetric model, resulting from both fewer elements from discretization and fewer Dofs by eliminating the fictitious frequency treatment. Compared to the conventional BEM solver, the FMBEM is much more efficient, which further reduces the computational cost. The combination of efficient FMBEM and thin shell modeling approach enables the use of the numerical method in the optimization framework. It is worth mentioning that the simulations can be conveniently run in parallel in the optimizer for multiple driving frequencies. Thus the total computational cost for a multi-frequency FMBEM on a thin shell model is fairly acceptable in practice. The modeling error and improvement of the thin shell model are discussed in the following Sections 3.2.4 and 3.2.5.

3.2.4. Size effect and error analysis

Compared to the volumetric model, the thin shell model has demonstrated a significant speedup in computational efficiency. Now the question is whether this model simplification induces large modeling errors on the acoustic field. To evaluate the accuracy, the relative error on the total acoustic pressure between a thin shell model (denoted as $\mathbb{S}$) and a full volumetric model (denoted as $\mathbb{V}$) is defined as

$$\epsilon_k(f, \mathbf{r}) = \frac{|P_{\mathbb{S},k}(f, \mathbf{r}) - P_{\mathbb{V},k}(f, \mathbf{r})|}{|P_{\mathbb{V},k}(f, \mathbf{r})|} \times 100\%, \quad k \in \{\text{flat, wavy}\}. \tag{11}$$

Fig. 4 presents the relative error for a flat profile and a wavy profile with three spatial sinusoidal components (parameter values are given in Table 1). The relative error is observed to be frequency dependent. In both flat and wavy profiles, the thin shell model demonstrates a relatively high error at relatively low frequencies, e.g., 4 kHz–6 kHz. Comparing the two colormaps, the relative error is also found to be profile dependent.
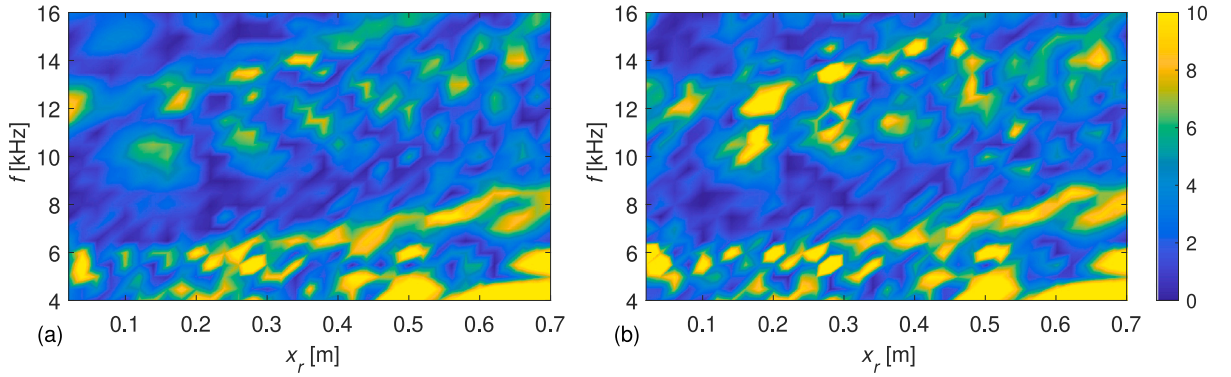
Fig. 4. Direct comparison of relative error [%] between volumetric model and thin shell model: (a) flat profile; (b) wavy profile. (For interpretation of the references to color in this figure legend, the reader is referred to the web version of this article.)

Fig. 5 presents a detailed comparison of the magnitude of the complex sound pressure at various driving frequencies. Similarly to Fig. 4, the differences between the thin shell and volumetric models are significant at low driving frequencies and at receivers towards the end of the panel. This can be observed in both flat and wavy profiles. As expected, the wavy profile provides a pressure curve with more fluctuations compared to the flat profile, which becomes more obvious as the frequency increases. Besides, the differences between the flat and wavy profiles are less significant at low frequencies. This can be problematic for the solution of the inverse problem as similar field pressure curves entail non-unique solutions. It should be noted that the pressure responses from flat and wavy profiles become very similar at some receiver points. This is particularly obvious towards the lateral edge of the panel and beyond ($x_r > 0.5$ m). For instance, at 4 kHz, the pressure responses between flat and wavy profiles become very similar starting from $x_r = 0.4$ m. This phenomenon becomes less visible as the frequency increases. At 14 kHz, the difference between flat and wavy profiles is obvious which indicates that all receivers can provide useful information for characterization. It should be noted that such a study can be useful for the design and determination of the microphone array in the measurement setup.

In addition, the phase information of the complex sound pressure is studied and shown in Fig. 6. As observed, the phase differences between flat and wavy profiles as well as for thin shell and volumetric models are negligible. This is perhaps due to the small geometry variation on the wavy profile and relatively low driving frequencies of interest. Thus, the present study only considers the phase-less acoustic responses.

3.2.5. Subtraction method and error analysis

As observed in a direct comparison with the volumetric model, the thin shell model may yield a large error (e.g. more than 10% for some frequencies at some microphone positions) due to the simplification of the panel volume. In order to mitigate this modeling error, a subtraction method is considered here. The idea is to subtract the field response obtained with the unknown surface from the one obtained with a known surface. In the present study, we consider rough surfaces with small roughness scales, e.g. Table 1. Thus it is reasonable to use a flat surface as the known surface. Besides, the incident field, as part of the acoustic response recorded by the microphones, may affect the characterization under certain circumstances. For instance, if the incident field dominates, the acoustic response at the microphones may become similar for different surface profiles. With the subtraction method, the incident field from the source is also eliminated here in the BEM simulation. In a measurement setup, the incident field can be mitigated by adjusting the source orientation and microphone positions [1]. The absolute pressure difference between an "unknown" surface (e.g. wavy profile in this case) and a "known" surface (e.g. flat profile in this case) is defined as

$$\Delta_l(f, \mathbf{r}) = | P_{\text{unknown},l}(f, \mathbf{r}) | - | P_{\text{known},l}(f, \mathbf{r}) |, \quad l \in \{\mathbb{S}, \mathbb{V}\}. \tag{12}$$

Fig. 7 presents the absolute pressure difference between wavy and flat profiles for the thin shell model and the volumetric model at various driving frequencies. It can be observed that the pressure difference between a thin shell and volumetric models becomes much smaller as compared to the direct evaluation in Fig. 5. The subtraction method has greatly eliminated the effects of the finite size. It can be found that the pressure difference is close to zero when the receiver is approaching the end of the panel and beyond ($x_r > 0.5$ m) at low driving frequencies. This is consistent with what has been discussed in Section 3.2.4. The root-mean-square error (RMSE) between the thin shell and volumetric model is given as

$$RMSE = \sqrt{\frac{1}{M} \sum_{i=1}^{M} (\gamma_{\mathbb{S},i} - \gamma_{\mathbb{V},i})^2}, \tag{13}$$

where γ is either the pressure P in a direct manner, or the pressure difference Δ in the subtraction method (as described in Eq. (12)). Fig. 8 presents the RMSE between the thin shell and volumetric models for the subtraction method and direct calculations of flat and wavy profiles. It is demonstrated that the subtraction method can significantly reduce the RMSE for the thin shell model over all the driving frequencies. The size effect of the finite sample is greatly mitigated in this way. The reduction at relatively low
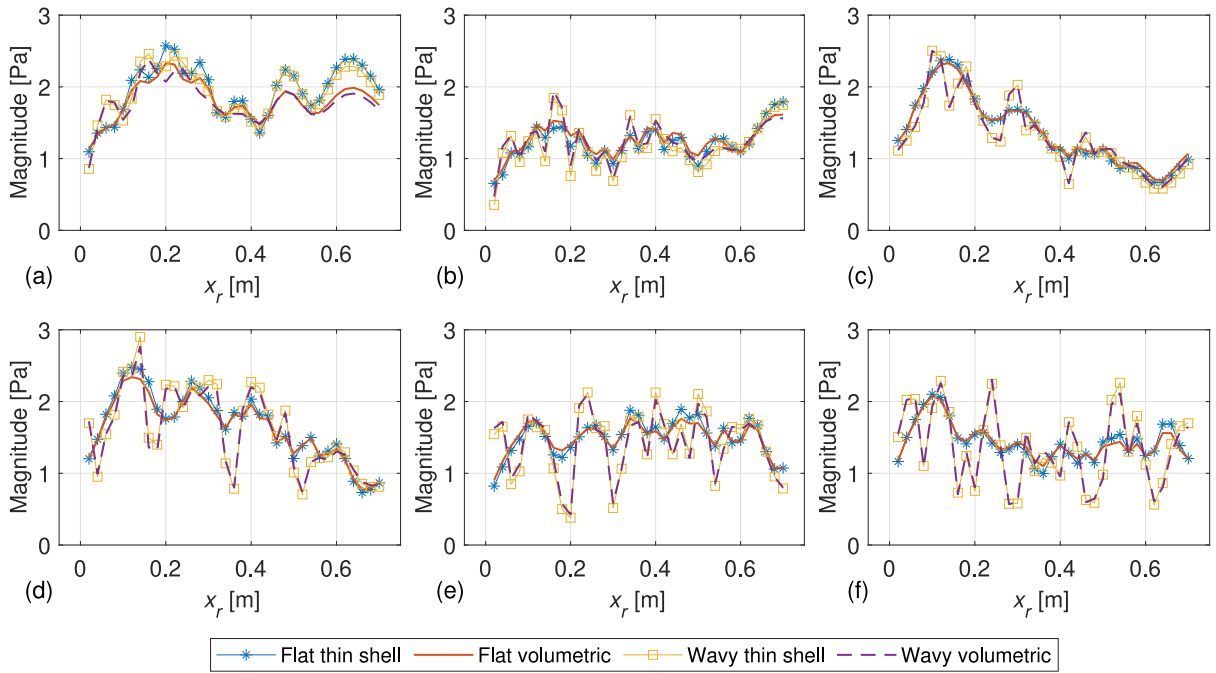
Fig. 5. Direct comparison of the field pressure of the flat and wavy profile using thin shell and volumetric models at various driving frequencies: (a) f = 4 kHz; (b) f = 6 kHz; (c) f = 8 kHz; (d) f = 10 kHz; (e) f = 12 kHz; (f) f = 14 kHz.
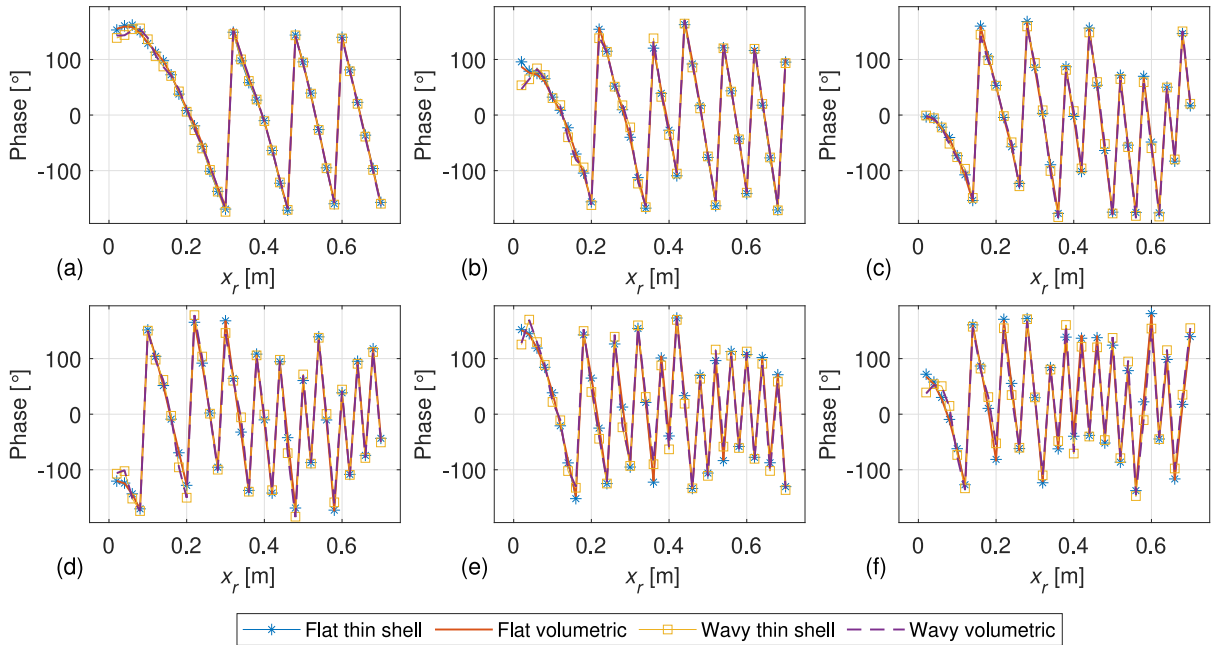

Fig. 6. Direct comparison of the acoustic phase of the flat and wavy profile using thin shell model and volumetric model at various driving frequencies: (a) f = 4 kHz; (b) f = 6 kHz; (c) f = 8 kHz; (d) f = 10 kHz; (e) f = 12 kHz; (f) f = 14 kHz.

frequencies i.e. $f \leq 7$ kHz makes the thin shell model eligible to use such frequencies for efficient and accurate inversion in later discussions. The size effect is independent of the surface impedance [50], therefore the subtraction method can also be used for surface impedance characterization. The "known" profile can be defined with a known surface shape or known surface impedance depending on the availability of the information.
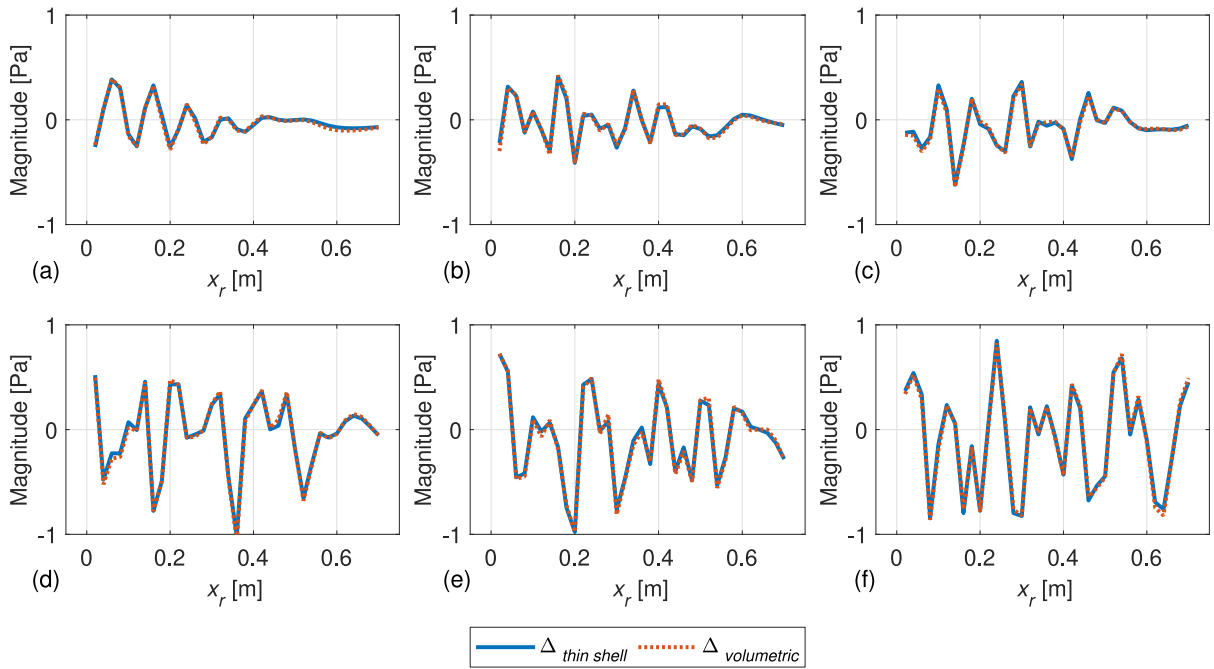
Fig. 7. Absolute pressure difference between wavy and flat profiles computed via subtraction method i.e. Eq. (12) for thin shell and volumetric models at various driving frequencies: (a) f = 4 kHz; (b) f = 6 kHz; (c) f = 8 kHz; (d) f = 10 kHz; (e) f = 12 kHz; (f) f = 14 kHz.
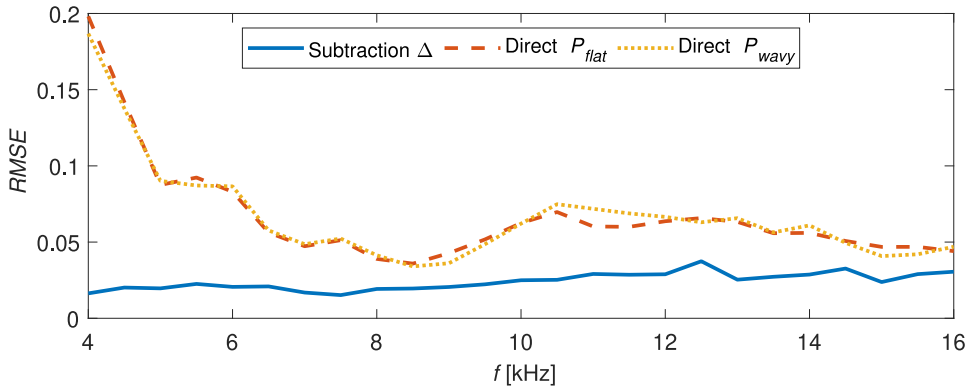

Fig. 8. RMSE between thin shell model and volumetric model for direct flat profile, wavy profile, and subtraction method at driving frequencies 4 kHz–16 kHz with 0.5 kHz resolution.

3.2.6. Adaptive geometry discretization for accurate characterization

In the characterization framework, the surface properties are updated iteratively, which may expose discretization errors for certain configurations. In the characterization of surface impedance, the surface shape is known *a priori* and thus has less concern about discretization error. As a general engineering rule of thumb, at least six linear elements are used to discretize the minimum acoustic wavelength. Based on the chosen frequencies, the element size can be determined *a priori*.

However, accurate geometry representation has to be considered when the surface shape is involved in the characterization as the geometry varies over iterations. A straightforward idea is to estimate the minimum surface variation and use a globally small element size in the characterization framework. However, this choice can be over-conservative, which leads to a computationally expensive BEM model for all the iterations. Instead, an adaptive discretization process is created in the inversion framework to reduce the computational cost while maintaining a sufficient accuracy level. More specifically, an *h*-refinement study is conducted firstly to evaluate the discretization error. For the rough surfaces that have been considered in this study, the surface elevation is comparably smaller than the geometric wavelength. Thus the ratio between the geometric wavelength and element length, i.e., the number of elements per geometric wavelength, is considered the metric for the investigation. Fig. 9 presents the results of a single sinusoidal surface at various driving frequencies. The relative L_2 errors ($\|P - P_{ref}\|_2 / \|P_{ref}\|_2$) are computed over all microphones using a reference case with considerably fine discretization (i.e., 31 elements per surface geometric wavelength). It can be observed
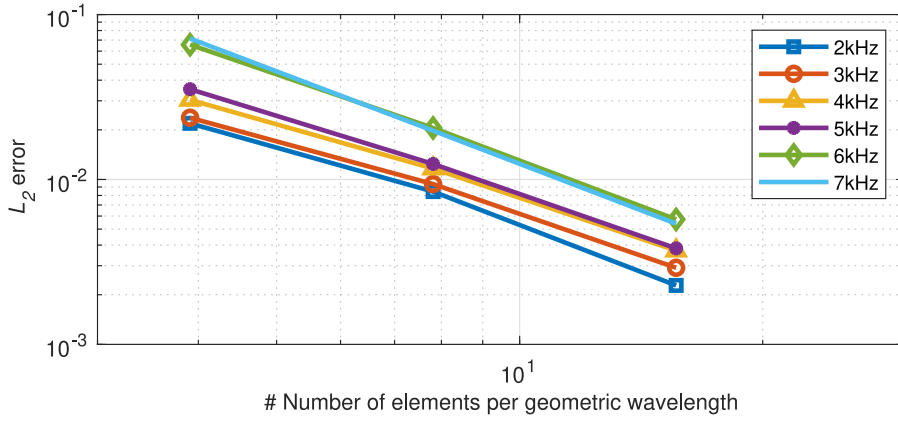
Fig. 9. h-refinement study for the surface geometry discretization.

that the L_2 error is slightly larger at high frequencies for a constant discretization. This aligns with the discretization error of acoustic waves, that is, lower acoustic frequencies benefit from a finer discretization thus providing higher accuracy. For the same frequency, finer discretization results in higher accuracy. This is an improvement due to both finer geometric and acoustic discretization. For a general engineering purpose, the use of ten elements per surface geometric wavelength, providing roughly 1% error, is considered sufficient in the frequency range of interest in terms of both efficiency and accuracy.

Thus, the element length h_{element} in the inversion framework is determined based on the considerations of both surface geometric wavelength and acoustic wavelength, which is

$$h_{\text{element}} = \min(\lambda_{\text{acoustic}}/6, \lambda_{\text{geometry}}/10). \tag{14}$$

The two constants can be adjusted according to the accuracy requirement and the maximum driving frequency. In the case of multiple sinusoidal components presented in the geometric shape, the smallest geometric wavelength is considered in Eq. (14). To minimize the discretization error among different surface profiles, this criterion is implemented and applied to every iteration of the shape estimation thus providing an adaptive geometry discretization in the characterization framework.

3.3. Additive signal noise

Considering the fact that noise appears in the measurement, the experimental signal-to-noise ratio (SNR) plays a significant role in obtaining acoustic signals with sufficient quality. Other uncertainties such as the non-smoothness of the surface could also be considered as an additional noise to the response signal. For simplicity, a global uncorrelated additive white Gaussian noise (AWGN) is considered and added to the synthetic acoustic signals for each microphone, as

$$P_n(f, \mathbf{r}) = P(f, \mathbf{r}) + \chi \cdot \sigma_P \cdot 10^{-\text{SNR}/20}, \tag{15}$$

where $P_n(f, \mathbf{r})$ and $P(f, \mathbf{r})$ are the signals with and without additive noise, χ is a zero-mean Gaussian distributed random variable with unit variance, σ_P is the standard deviation of the signal without additive noise.

Three SNRs (10 dB, 20 dB, and 30 dB) are considered and their corresponding AWGNs are added to the acoustic signals respectively. Section 4.1.1 investigates the effects of using different SNRs on the characterization.

4. Examples of surface characterization

This section presents examples and discussions of rough surface characterization. The study consists of surface impedance characterization using single- and multiple-parameter porous models, and surface shape characterization using multiple spatial sinusoidal components. It is worth noting that, owing to the nature of the numerical model at hand, the surface is assumed to be locally reacting. Two simultaneous characterizations of surface impedance and shape are also presented. All the presented examples have similar configurations as shown in Fig. 1, and only consider the receivers at $y_r = 0$ in the characterization.

4.1. Surface impedance characterization

The standardized methods for surface impedance measurement typically require a sample of the target material [14,51]. The selected sample is expected to be representative of the target material, which sometimes can be difficult to verify. The present characterization framework can be of interest as an alternative non-destructive mean for surface impedance characterization *in situ*.

The surface shape in this section is assumed to be known as flat. The surface impedance is considered to be estimated/modeled by phenomenological porous material models as described in Section 3.1. Two examples are presented using single- and multiple-parameter porous material models respectively. The driving frequencies are selected to ensure an efficient calculation in FMBEM and to capture the characteristics of the impedance as much as possible.

Table 3

Initial estimations and bounds for parameters in surface impedance characterization. The estimated values are obtained under AWGN with SNR = 20 dB. Abbreviation: "charac.len." is "characteristic length".

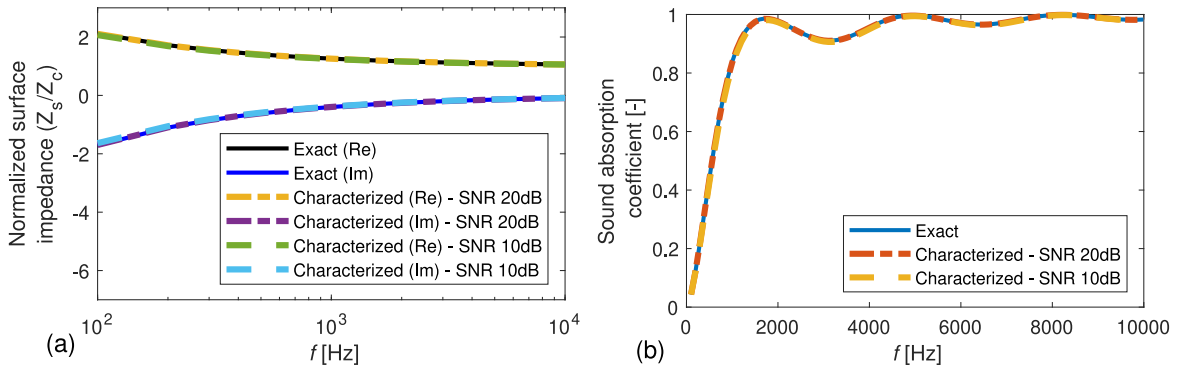| Model	Parameters	Initial	B^l	B^u	Increment	Target	Estimated
DBM	Flow resistivity [N s m^{-4}]	1000	100	200 000	10	8000	7910
JCA	Flow resistivity [N s m^{-4}]	1000	500	20 000	100	4067	16 400
	Porosity [–]	0.7	0.5	1	0.01	0.62	0.61
	Tortuosity [–]	2	1	5	0.1	2.17	2.20
	Viscous charac.len. [μm]	150	50	350	3.4	165.9	156.2
	Thermal charac.len. [μm]	150	50	350	3.4	210.6	285.4

Fig. 10. Characterization of surface impedance using DBM model. (a) compares the "exact" and "characterized" normalized surface impedance; (b) compares the "exact" and "characterized" absorption coefficient. The "characterized" results with SNR = 30 dB are the same as the "exact" in this case, which are not shown in the figure.

4.1.1. Characterization using a single-parameter model

In the study of the single-parameter case, the DBM model is employed to estimate the surface impedance. The thickness of the panel is assumed to be known e.g., 50 mm, whereas the static air flow resistivity is to be determined. The material is considered to be backed by a rigid surface. We consider four driving frequencies, 1 kHz, 2 kHz, 3 kHz and 4 kHz respectively. From the analysis in Section 3.2.5, it has been found that the microphones towards the lateral end of the sample may not provide useful information at low frequencies. Thus, a reduced number, i.e., 21 of microphones is used in this case which covers a distance range of 400 mm. The driving frequencies are selected such that sufficient field data are available for inversion and determination of the unknown parameter. The upper and lower bounds of the parameters listed in Table 3 are defined as large to cover a wide range of possibilities. For simplicity, the flow resistivity of the DBM model within the bounds follows a discrete uniform distribution with an increment of 10 N s m^{-4}, giving a search space of size 19 991. In practice, the decision of variation range and distribution function could be based on the *a priori* knowledge of the surface. In this case, the synthetic data is generated using a flow resistivity of $\sigma = 8000$ N s m^{-4}. In addition, AWGN with three SNRs is considered for the synthetic data to evaluate the robustness of the characterization framework. The selections of SNR cover a range from a relatively poor signal quality of 10 dB to a good signal quality of 30 dB.

As a result, the estimated flow resistivity (with the smallest CF residual) is 7470 N s m^{-4}, 7910 N s m^{-4}, 8000 N s m^{-4} for the inversions using SNRs of 10 dB, 20 dB, and 30 dB respectively. With the best SNR of 30 dB, the inversion framework manages to retrieve the exact input. In the inversions with SNRs of 10 dB and 20 dB, the target flow resistivity (i.e. 8000 N s m^{-4}) is in fact captured by the optimizer, however, the CF residual with the target value is slightly higher than that with the final estimated value. It seems that the AWGN has shifted the acoustic signals closer to the ones obtained from other vicinal inputs, which leads to confusion about the optimizer. The L_2 norm of the corresponding complex impedance, computed as $\epsilon_Z = \| Z - Z_{\text{ref}} \|_2 / \| Z_{\text{ref}} \|_2$, are 0.0022 and 0.0131 for SNR of 20 dB and 10 dB. The RMSE of absorption coefficient, computed as $\epsilon_\alpha = \sqrt{\sum_{i=1}^{M} (\alpha - \alpha_{\text{ref}})/M}$, are 0.0009 and 0.0056 for SNR of 20 dB and 10 dB. A comparison of the complex impedance and absorption coefficient are given in Fig. 10. The assessment of the inversion quality depends on the output of interest. For instance, if the objective is to estimate the complex impedance curve (or absorption coefficient), the inversions from all of the three SNRs are considered fine with a maximum error of 0.0131 (or 0.0056 for absorption coefficient) at SNR = 10 dB. On the other hand, if the objective is to estimate the flow resistivity of the DBM model, the inversion using a high SNR, such as 20 dB (or 30 dB), would provide a close estimation with a relative error of 1.13% (or 0.0% for SNR = 30 dB) in the present case. With the consideration from actual experiments e.g. in a semi-anechoic chamber and/or using time averaging of the measured responses, the SNR of 20 dB is reasonable to obtain in practice. Thus, it is applied to all the remaining synthetic data.

4.1.2. Characterization using a multiple-parameter model

As a general equivalent fluid model, the JCA model has been widely used to describe porous materials in practice. In this case study, a wood-wool cement board is considered, likewise in a rigid backing configuration. The JCA model has been evaluated
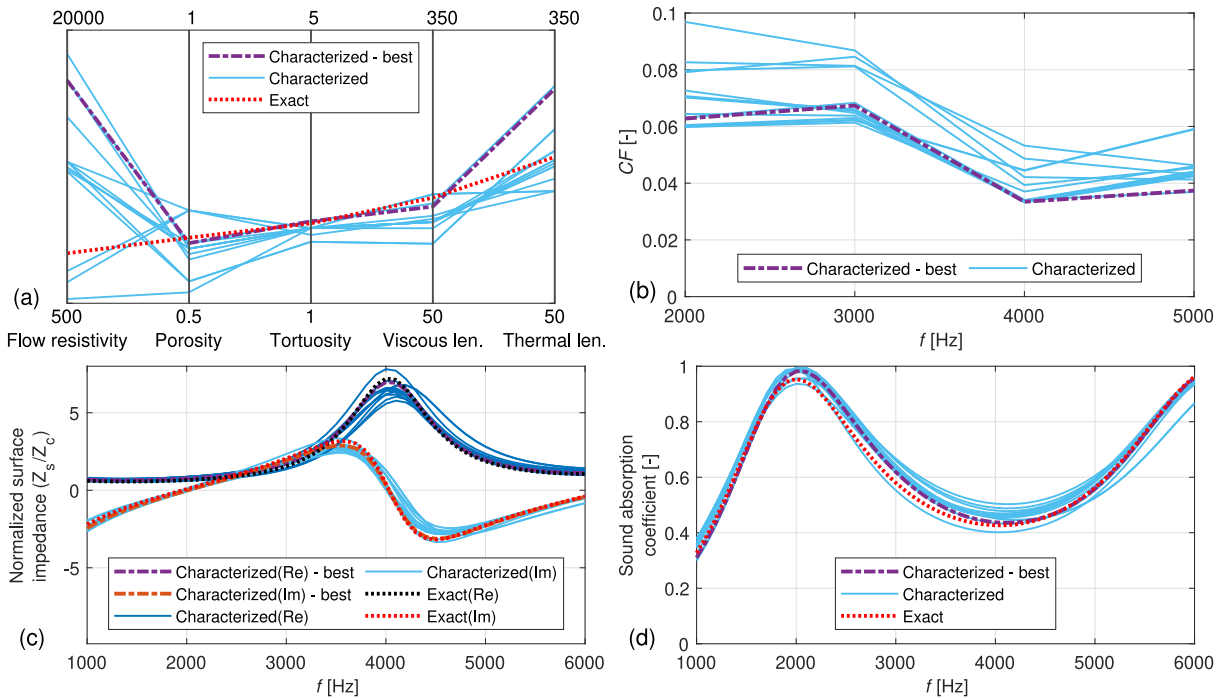
Fig. 11. Characterization of surface impedance using JCA model. (a) compares the JCA parameters from 15 selected characterizations; (b) shows the CF residuals for the 15 selected characterizations; (c) compares the resulting normalized surface impedance from the characterizations; (d) compares the absorption coefficients from the characterizations.

experimentally in characterizing such material [41,52]. Given the thickness, the classical JCA model consists of five parameters. The same parameter ranges from literature [52] are applied to the present inversion study as shown in Table 3. The search space for the optimizer contains 4.18 billion parameter combinations. It should be mentioned that the static flow resistivity was measured separately in the cited work using the standard measurement technique [53]. In the present work, the static flow resistivity is intended to maintain as unknown similar to other parameters. Its upper and lower bounds are chosen sufficiently large to cover the typical range of this particular material. It is of relevance to investigate whether all the phenomenological parameters can be retrieved from a single inversion setup.

Four driving frequencies including 2 kHz, 3 kHz, 4 kHz and 5 kHz are selected in this case. For each parameter in the JCA model, Table 3 lists the best-estimated value compared to the target. The porosity, tortuosity, and viscous characteristic length have been well estimated by the framework, while the flow resistivity and thermal characteristic length seem to yield large differences. We further analyze the 15 best designs from the optimizer. The parameters of these sets are plotted in Fig. 11(a). The flow resistivity and the thermal characteristic length do not converge within the maximum number of iterations. In particular, due to the choice of relatively high frequencies in the example chosen here, the material impedance approaches its asymptotic behavior and therefore exhibits low sensitivity to the flow resistivity, leading to an apparent non-uniqueness of the solution. The other three parameters seem to converge to the vicinity of the ground truth. On the other hand, most of the sets seem to give similar CF residuals as shown in Fig. 11(b). The best characterization maintains an overall minimum CF value (by linearly averaging the final CF values over all the frequencies). The resulting complex impedance and corresponding absorption coefficients are compared in Fig. 11(c) and (d). All the designs give close estimations of the ground truth. With the best estimation, the L_2 error of complex impedance is computed to be 0.0509 and the RMSE of the absorption coefficient is 0.0238. Similar to the single-parameter impedance characterization case, the assessment of the inversion quality depends on the output of interest. If the primary objective is to estimate the impedance/absorption coefficient curve, the proposed framework seems to return good quality estimation using the current stopping criteria. In the present case, the flow resistivity is the most challenging parameter to estimate for the optimizer. The large range of values in the obtained flow resistivity indicates that the scattered field is insensitive to this parameter in the studied case. If an accurate estimation of the parameter value is required, a more stringent stopping criterion could possibly help to obtain a better estimation, which also requires more computational efforts. Besides, using a multiple-parameter model with less number of parameters, e.g. the three-parameter model proposed by Horoshenkov et al. [54], may also improve the quality of the characterization.
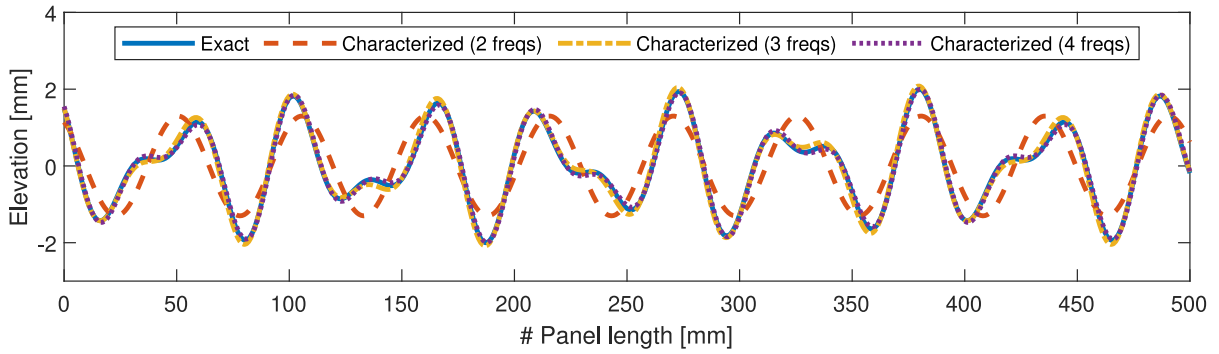
Fig. 12. Surface shape characterizations using different numbers of driving frequencies. "freqs" stands for "frequencies".

Table 4
Initial estimations and bounds for shape characterization.

Parameters	Symbol	Initial	B^l	B^u	Increment
Amplitude [mm]	z_n	0.5	0	2	0.1
Wavelength [mm]	λ_n	100	30	200	10
Phase [rad]	ϕ_n	0.1	0	2	0.1

4.2. Surface shape characterization

In the rough surface shape characterization, the surface is assumed to be perfectly rigid. This is a fair assumption in practice when the speed of sound is significantly larger than that in the medium above (e.g., observing a water surface from the air). A rough surface model from Eq. (10) with two sinusoidal components is considered here. The parameter bounds are given in Table 4. In this case, the search space consists of approximately 63 million parameter combinations. It should be noted that the actual search space is nearly half considering the equivalence of the two sinusoidal components. This is not taken into consideration in the present framework.

In order to avoid an under-determined problem (thus non-unique solutions), sufficient input information shall be generated for the inversion. The number of such inputs is determined by the number of driving frequencies in the forward modeling. The selected driving frequencies should also be able to capture the geometric variation of the surface roughness. In the impedance characterization, multiple frequencies are used by default considering the dependence of surface impedance on frequency. For surface characterization, it is relevant to investigate the effects of the number of frequencies on the characterization quality. Thus, different numbers of frequencies are defined in this case. Three settings are considered using two (i.e. 5 kHz and 6 kHz), three (i.e. 4 kHz, 5 kHz, and 6 kHz) and four driving frequencies (i.e. 4 kHz, 5 kHz, 6 kHz and 7 kHz) respectively. The multi-frequency simulations are processed in parallel using the same hardware with a four-core CPU as before. More driving frequencies could be considered if hardware allows.

The estimated results with the minimum *CF* values in each optimization are compared in Fig. 12. Dividing the RMSE by the maximum amplitude of the exact surface profile, the relative root-mean-square error (rRMSE) is computed as 0.2868, 0.0446, 0.0288 for the cases of two, three, and four driving frequencies respectively. By using two driving frequencies, the inversion yields a large deviation within the maximum iteration number. This indicates that the input information is not sufficient to reconstruct the shape. In the case of three and four driving frequencies, the surface shape is characterized well with fewer noticeable errors. Using four driving frequencies gives the most accurate characterization, which confirms that more input in terms of driving frequencies helps to obtain high characterization quality. The accuracy level is considered to be acceptable with four driving frequencies in the present study.

4.3. Simultaneous characterization of surface impedance and shape

In a complex setup, both surface impedance and shape are unknown and expected to be characterized by the inversion framework. Such cases are relevant for instance in *in situ* material characterizations for porous materials with rough surfaces, such as absorptive foam with thickness variations, sound absorption curtains, etc.

In the following simultaneous characterization, two examples are investigated and presented. The "known" surface in this discussion is a rigid flat surface. The "unknown" absorptive surface shapes are described by either one or two sinusoidal components from Eq. (10) with bounds from Table 4. For simplicity, the DBM model is considered in the surface impedance for both cases. The flow resistivity ranges from 100 N s m^{-4} to 20 000 N s m^{-4} with 220 variations. Therefore, the search space becomes approximately 1.7 million for the case with one sinusoidal component and 13.86 billion for the case with two sinusoidal components. The synthetic data is generated by using a flow resistivity of 8650 N s m^{-4}, in a 50 mm-thick rigid-backed configuration. An AWGN with 20 dB SNR
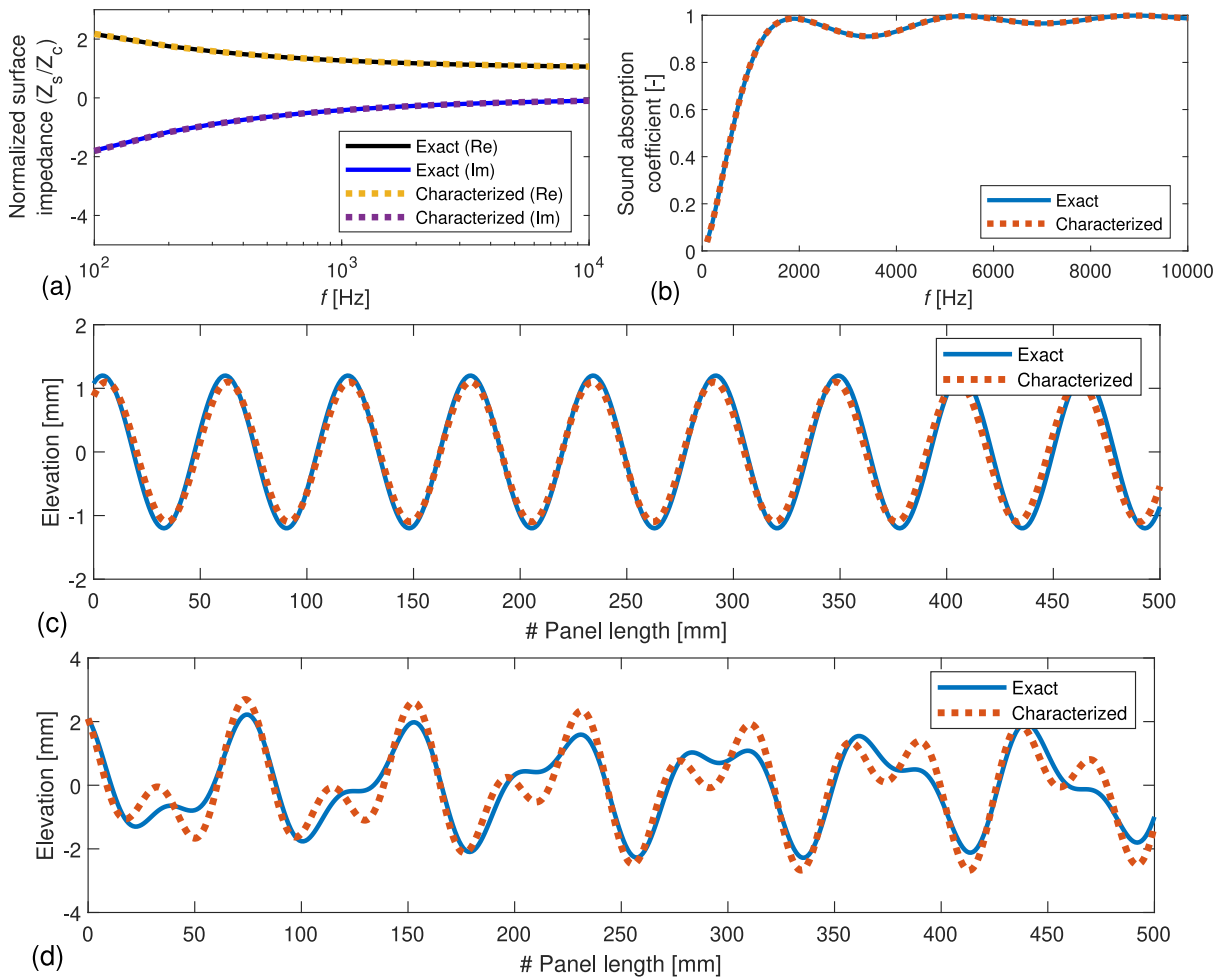
Fig. 13. Characterization of rough surface in terms of impedance and shape. (a) compares the normalized surface impedance; (b) compares the corresponding absorption coefficients; (c) compares the characterized surface shape using one sinusoidal component; (d) compares the characterized surface shape using two sinusoidal components. The estimated surface impedance values are identical for surface profiles with one and two sinusoidal components.

is added to all the synthetic data. Four driving frequencies (4 kHz, 5 kHz, 6 kHz, and 7 kHz) are used in parallel in the framework. Considering the large size of the search space, especially in the case of two sinusoidal components, an enlarged iteration number of 3000 is used in the optimizer for both characterizations.

Fig. 13 shows the results of the two characterization cases. The estimated flow resistivity is obtained in both cases as 8732.4 N s m^{-4}, which is close to the ground truth with a relative difference of 0.0095. Compared to the reference impedance curve, the L_2 error of complex impedance is 0.0019 and the RMSE of the absorption coefficient is 0.0008. In terms of surface shape, the estimated shape of the case with one component is close to the exact reference, with an rRMSE of 0.114. With two components involved in the surface shape, the number of unknowns increases from 4 to 7. As shown in Fig. 13(d), the estimated shape describes the main behavior of the exact reference. The large geometric wave has been captured well, while deviations are observed on the smaller geometric waves. The rRMSE of the characterized shape is computed as 0.2294 with respect to the exact reference. The surface shape in the case with two sinusoidal components becomes more challenging to estimate due to the increased number of unknowns which exponentially expands the search space. The case with more unknowns leads to slightly larger errors in the estimated shape. In both cases, the surface impedance has been well estimated using the single-parameter model.

To further improve the quality of the characterization, several aspects could be explored. As discussed, the performance of the optimizer depends on the size of the search space. The selection of the phenomenological model is thus important for the optimization. Using a smaller number of unknowns can significantly reduce the size of the search space. It is also useful to provide a more precise value range for each unknown involved in the optimizer. Both aspects may require some *a prior* understanding of the unknown surface. Besides, using multiple frequencies may increase the accuracy of the characterization by including more inputs to the inverse problem. In addition, stringent stopping criteria could also improve the quality of the characterization, but would substantially increase the computational time. A general-purpose optimizer is being used in the present work, other types of optimizers could be relevant to test for optimal performance.

5. Discussion and conclusion

This paper presents a multi-frequency characterization framework using acoustic simulations and optimizations to characterize rough surfaces in terms of surface impedance and/or surface shape. A thin shell modeling approach has been proposed to simplify the modeling and simulation of the acoustic scattering problem using an indirect FMBEM. It has been demonstrated that the indirect FMBEM solver and the proposed thin shell model provide significant improvement in computational efficiency as compared to the conventional BEM and a volumetric representation of the problem. The combination of the two enables the use of the BEM in rough surface characterization. The finite size of the surface is also considered by the FMBEM solver. The size effect from the surface sample is analyzed to quantify the modeling error. A subtraction method is proposed to mitigate the surface modeling error, which also enables the use of relatively low driving frequencies (compared to the roughness scale) in the characterization. A discretization criterion that concerns both acoustic and geometric aspects is proposed for surface shape characterization in order to maintain an acceptable discretization error in the iterations of the optimization loop.

In the characterization of surface impedance, both single-parameter (i.e. DBM) and multiple-parameter (i.e. JCA) porous material models are considered. It is observed that the proposed framework can characterize the surface with a certain noise level (e.g. SNR of 20 dB). Due to the choice of relatively high driving frequencies, where the porous material impedance reaches an asymptotic behavior independent from flow resistivity, the characterization methodology exhibits low sensitivity to this parameter. Nevertheless, the impedance is well reconstructed. Indeed, the method provides accurate results with a RMSE of 0.0009 on the absorption coefficient for a single-parameter model and a RMSE of 0.0238 for a model with multiple parameters. In the characterization of surface shape, it is observed that more driving frequencies lead to a higher characterization quality. A RMSE of 0.0288 is obtained for a surface with two sinusoidal components when using four driving frequencies in parallel. Two cases are presented for the simultaneous characterization of surface shape and impedance using the DBM model. The case with more unknowns on the surface shape leads to larger estimation errors on the final characterization. On the other hand, the surface impedance has been retrieved well in both cases. It is worth noting that the DBM model involves flow resistivity as the sole unknown. The use of a more complex porous material model may hinder the estimation of both impedance and shape as the search space increases exponentially with the number of unknowns.

The present framework is considered to be applicable to a wide range of continuous rough surfaces, whose properties can be described or estimated by phenomenological impedance models and/or shape functions. Such parameterization can be defined based on the *a priori* information of the target surface. Other types of surfaces e.g. pyramidal wedges could be relevant to investigate in the future. In the present work, the same numerical model is used for both the reference data and the estimation. The existence of an inverse crime scenario has been mitigated by the incorporation of additive noise in the reference data and the inverse problem is observed to be non-trivial even in a well-controlled environment. To achieve the optimal quality from the framework, it is also relevant to test the setup in a massive way, e.g. using the Monte-Carlo method to investigate the relevant aspects such as various porous materials, the position and the number of microphones. The future work will also focus on the design of a test rig based on the insights obtained from the simulations in the present work. A measurement validation will be conducted to further verify the robustness of the proposed framework.

CRediT authorship contribution statement

Yue Li: Conceptualization, Methodology, Software, Validation, Formal analysis, Investigation, Data curation, Visualization, Writing – original draft, Writing – review & editing. **Jacques Cuenca:** Methodology, Formal analysis, Investigation, Writing – review & editing. **Laurent De Ryck:** Resources, Investigation, Writing – review & editing. **Mansour Alkmim:** Resources, Investigation, Writing – review & editing. **Onur Atak:** Resources, Writing – review & editing. **Wim Desmet:** Resources, Writing – review & editing. **Giulio Dolcetti:** Resources, Investigation, Writing – review & editing. **Anton Krynkin:** Resources, Investigation, Writing – review & editing.

Declaration of competing interest

The authors declare that they have no known competing financial interests or personal relationships that could have appeared to influence the work reported in this paper.

Data availability

Data will be made available on request.

References

[1] G. Dolcetti, M. Alkmim, J. Cuenca, L. De Ryck, A. Krynkin, Robust reconstruction of scattering surfaces using a linear microphone array, J. Sound Vib. 494 (2021) 115902.

[2] L. Hellequin, J.-M. Boucher, X. Lurton, Processing of high-frequency multibeam echo sounder data for seafloor characterization, IEEE J. Ocean. Eng. 28 (1) (2003) 78–89.

[3] J.T. Johnson, R.J. Burkholder, J.V. Toporkov, D.R. Lyzenga, W.J. Plant, A numerical study of the retrieval of sea surface height profiles from low grazing angle radar data, IEEE Trans. Geosci. Remote 47 (6) (2008) 1641–1650.

[4] A. Nichols, S. Tait, K. Horoshenkov, S. Shepherd, A non-invasive airborne wave monitor, Flow Meas. Instrum. 34 (2013) 118–126.

[5] S.P. Walstead, G.B. Deane, Reconstructing surface wave profiles from reflected acoustic pulses using multiple receivers, J. Acoust. Soc. Am. 136 (2) (2014) 604–613.

[6] G. Dolcetti, A. Krynkin, K.V. Horoshenkov, S.J. Tait, An acoustic technique to measure the velocity of shallow turbulent flows remotely, in: M. Kalinowska, M. Mrokowska, P. Rowinski (Eds.), Free Surface Flows and Transport Processes, GeoPlanet: Earth and Planetary Sciences, Springer, 2018, pp. 181–194.

[7] D.L. Colton, R. Kress, Inverse Acoustic and Electromagnetic Scattering Theory, Vol. 93, Springer, 1998.

[8] R. Wombell, J.A. DeSanto, The reconstruction of shallow rough-surface profiles from scattered field data, Inverse Problems 7 (1) (1991) L7.

[9] A. Krynkin, K.V. Horoshenkov, T. Van Renterghem, An airborne acoustic method to reconstruct a dynamically rough flow surface, J. Acoust. Soc. Am. 140 (3) (2016) 2064–2073.

[10] R. Coifman, M. Goldberg, T. Hrycak, M. Israeli, V. Rokhlin, An improved operator expansion algorithm for direct and inverse scattering computations, Waves Random Media 9 (3) (1999) 441.

[11] M. Stankova, J. Burov, M. Burova, Computer reconstruction of a periodic surface by means of the scattered and transmitted acoustic fields, Meas. Sci. Technol. 12 (8) (2001) 1330.

[12] M. El-Shenawee, E.L. Miller, Multiple-incidence and multifrequency for profile reconstruction of random rough surfaces using the 3-D electromagnetic fast multipole model, IEEE Trans. Geosci. Remote 42 (11) (2004) 2499–2510.

[13] A. Schatzberg, A.J. Devaney, Rough surface inverse scattering within the Rytov approximation, J. Opt. Soc. Amer. A 10 (5) (1993) 942–950.

[14] International Organization for Standardization, ISO 10534-2:1998. Acoustics — Determination of sound absorption coefficient and impedance in impedance tubes — Part 2: Transfer-function method, Geneva, 1998.

[15] International Organization for Standardization, ISO 354:2003. Acoustics — Measurement of sound absorption in a reverberation room, Geneva, 2003.

[16] M. Niskanen, J.-P. Groby, A. Duclos, O. Dazel, J. Le Roux, N. Poulain, T. Huttunen, T. Lähivaara, Deterministic and statistical characterization of rigid frame porous materials from impedance tube measurements, J. Acoust. Soc. Am. 142 (4) (2017) 2407–2418.

[17] F. Pompoli, P. Bonfiglio, K.V. Horoshenkov, A. Khan, L. Jaouen, F.-X. Bécot, F. Sgard, F. Asdrubali, F. D'Alessandro, F. Hübelt, et al., How reproducible is the acoustical characterization of porous media? J. Acoust. Soc. Am. 141 (2) (2017) 945–955.

[18] E. Brandão, A. Lenzi, S. Paul, A review of the in situ impedance and sound absorption measurement techniques, Acta Acust. United Acust. 101 (3) (2015) 443–463.

[19] C. Chien, W. Soroka, Sound propagation along an impedance plane, J. Sound Vib. 43 (1) (1975) 9–20.

[20] C. Chien, W. Soroka, A note on the calculation of sound propagation along an impedance surface, J. Sound Vib. 69 (2) (1980) 340–343.

[21] T. Kawai, T. Hidaka, T. Nakajima, Sound propagation above an impedance boundary, J. Sound Vib. 83 (1) (1982) 125–138.

[22] X. Di, K.E. Gilbert, An exact Laplace transform formulation for a point source above a ground surface, J. Acoust. Soc. Am. 93 (2) (1993) 714–720.

[23] J.D. Alvarez, F. Jacobsen, An iterative method for determining the surface impedance of acoustic materials in situ, in: 37th International Congress and Exposition on Noise Control Engineering, 2008.

[24] Z.-W. Luo, C.-J. Zheng, Y.-B. Zhang, C.-X. Bi, Estimating the acoustical properties of locally reactive finite materials using the boundary element method, J. Acoust. Soc. Am. 147 (6) (2020) 3917–3931.

[25] M. Müller-Trapet, P. Dietrich, M. Aretz, J. van Gemmeren, M. Vorländer, On the *in situ* impedance measurement with *pu*-probes - Simulation of the measurement setup, J. Acoust. Soc. Am. 134 (2) (2013) 1082–1089.

[26] E. Brandão, E. Tijs, A. Lenzi, H.-E. de Bree, A comparison of three methods to calculate the surface impedance and absorption coefficient from measurements under free field or *in situ* conditions, Acta Acust. United Acust. 97 (6) (2011) 1025–1033.

[27] E. Brandão, A. Lenzi, J. Cordioli, Estimation and minimization of errors caused by sample size effect in the measurement of the normal absorption coefficient of a locally reactive surface, Appl. Acoust. 73 (6–7) (2012) 543–556.

[28] E. Zea, E. Brandão, M. Nolan, J. Andén, J. Cuenca, P. Svensson, Learning the finite size effect for in-situ absorption measurement, in: Euronoise 2021 (E-Congress), Madeira, Portugal, October 25-27, 2021, pp. 1477–1486.

[29] V. Twersky, Reflection and scattering of sound by correlated rough surfaces, J. Acoust. Soc. Am. 73 (1) (1983) 85–94.

[30] I. Tolstoy, Smoothed boundary conditions, coherent low-frequency scatter, and boundary modes, J. Acoust. Soc. Am. 75 (1) (1984) 1–22.

[31] P. Boulanger, K. Attenborough, Q. Qin, Effective impedance of surfaces with porous roughness: Models and data, J. Acoust. Soc. Am. 117 (3) (2005) 1146–1156.

[32] H.-H. Qin, H.-K. Pang, J.-C. Liu, Reconstruction for shape and impedance in an inverse scattering problem, Int. J. Comput. Math. 98 (5) (2021) 1015–1028.

[33] V. Rokhlin, Diagonal forms of translation operators for the Helmholtz equation in three dimensions, Appl. Comput. Harmon. Anal. 1 (1) (1993) 82–93.

[34] N. Chase, M. Redemacher, E. Goodman, R. Averill, R. Sidhu, A Benchmark Study of Optimization Search Algorithms, Red Cedar Technology, MI, USA, 2010, pp. 1–15.

[35] N. Vlahopoulos, Indirect variational boundary element method in acoustics, in: T. Wu (Ed.), Boundary Element Acoustics Fundamentals and Computer Codes, WIT Press, 2002, pp. 83–115.

[36] M. Fischer, The Fast Multipole Boundary Element Method and its Application to Structure Acoustic Field Interaction (Ph.D. thesis), University of Stuttgart, 2004.

[37] E. Darve, The fast multipole method: numerical implementation, J. Comput. Phys. 160 (1) (2000) 195–240.

[38] E. Darve, The fast multipole method I: error analysis and asymptotic complexity, SIAM J. Numer. Anal. 38 (1) (2000) 98–128.

[39] D.L. Johnson, J. Koplik, R. Dashen, Theory of dynamic permeability and tortuosity in fluid-saturated porous media, J. Fluid Mech. 176 (1987) 379–402.

[40] Y. Champoux, J.-F. Allard, Dynamic tortuosity and bulk modulus in air-saturated porous media, J. Appl. Phys. 70 (4) (1991) 1975–1979.

[41] Y. Atalla, R. Panneton, Inverse acoustical characterization of open cell porous media using impedance tube measurements, Can. Acoust. 33 (1) (2005) 11–24.

[42] J. Allard, N. Atalla, Propagation of Sound in Porous Media: Modelling Sound Absorbing Materials, John Wiley & Sons, 2009.

[43] Siemens Digital Industries Software, Simcenter HEEDS, Version 2021.1.0, 2021.

[44] Y. Miki, Acoustical properties of porous materials-modifications of Delany-Bazley models, J. Acoust. Soc. Jpn. 11 (1) (1990) 19–24.

[45] M. Delany, E. Bazley, Acoustical properties of fibrous absorbent materials, Appl. Acoust. 3 (2) (1970) 105–116.

[46] A. Krynkin, G. Dolcetti, S. Hunting, Acoustic imaging in application to reconstruction of rough rigid surface with airborne ultrasound waves, Rev. Sci. Instrum. 88 (2) (2017) 024901.

[47] J.-T. Chen, S. Lin, J. Tsai, Fictitious frequency revisited, Eng. Anal. Bound. Elem. 33 (11) (2009) 1289–1301.

[48] R. D'Amico, J. Neher, B. Wender, M. Pierini, On the improvement of the solution accuracy for exterior acoustic problems with BEM and FMBEM, Eng. Anal. Bound. Elem. 36 (7) (2012) 1104–1115.

[49] Siemens Digital Industries Software, Simcenter 3D, version 2021.2.0, 2021.

[50] N. Atalla, F. Sgard, C.K. Amedin, On the modeling of sound radiation from poroelastic materials, J. Acoust. Soc. Am. 120 (4) (2006) 1990–1995.

[51] International Organization for Standardization, ISO 13472-2:2010. Acoustics — Measurement of sound absorption properties of road surfaces in situ — Part 2: Spot method for reflective surfaces, Geneva, 2010.

[52] B. Botterman, G.D. de la Grée, M. Hornikx, Q. Yu, H. Brouwers, Modelling and optimization of the sound absorption of wood-wool cement boards, Appl. Acoust. 129 (2018) 144–154.

[53] International Organization for Standardization, ISO 9053-1:2018. Acoustics — Determination of Airflow Resistance — Part 1: static Airflow Method, Geneva, 2018.

[54] K.V. Horoshenkov, A. Hurrell, J.-P. Groby, A three-parameter analytical model for the acoustical properties of porous media, J. Acoust. Soc. Am. 145 (4) (2019) 2512–2517.